

# Radius, rotational period and inclination of the Be stars in the Be/gamma-ray binaries MWC 148 and MWC 656\*

R. K. Zamanov<sup>1, \*\*</sup>, K. A. Stoyanov<sup>1</sup>, J. Martí<sup>2</sup>, V. D. Marchev<sup>1</sup>, and Y. M. Nikolov<sup>1</sup>

<sup>1</sup> Institute of Astronomy and National Astronomical Observatory, Bulgarian Academy of Sciences, Tsarigradsko Shose 72, BG-1784 Sofia, Bulgaria

<sup>2</sup> Departamento de Física, Escuela Politécnica Superior de Jaén, Universidad de Jaén, Campus Las Lagunillas, A3, 23071, Jaén, Spain

Received 2020 November 3, accepted 2020 February 3

Published online ...

**Key words** Stars: emission-line, Be – binaries: spectroscopic – Gamma rays: stars – Stars: individual: MWC 148, MWC 656

Using TESS photometry and Rozhen spectra of the Be/ $\gamma$ -ray binaries MWC 148 and MWC 656, we estimate the projected rotational velocity ( $v \sin i$ ), the rotational period ( $P_{\text{rot}}$ ), radius ( $R_1$ ), and inclination ( $i$ ) of the mass donor. For MWC 148 we derive  $P_{\text{rot}} = 1.10 \pm 0.03$  d,  $R_1 = 9.2 \pm 0.5 R_{\odot}$ ,  $i = 40^{\circ} \pm 2^{\circ}$ , and  $v \sin i = 272 \pm 5$  km s<sup>-1</sup>. For MWC 656 we obtain  $P_{\text{rot}} = 1.12 \pm 0.03$  d,  $R_1 = 8.8 \pm 0.5 R_{\odot}$ ,  $i = 52^{\circ} \pm 3^{\circ}$ , and  $v \sin i = 313 \pm 3$  km s<sup>-1</sup>. For MWC 656 we also find that the rotation of the mass donor is coplanar with the orbital plane.

Copyright line will be provided by the publisher

## 1 Introduction

The  $\gamma$ -ray binaries are a recently established and rare subclass of the high-mass X-ray binaries with most of their luminosity output being radiated above 1 MeV (Dubus 2013; Chernyakova & Malyshev 2020). They are composed of an OBe donor star and a neutron star or a black hole (Mirabel 2012). The mechanism responsible for the high-energy emission in these systems is still a subject of debate. The  $\gamma$ -rays could be produced either by accretion-driven jets, or by the rotation-powered strong pulsar winds interacting with the nearby medium (Dubus 2006; Romero et al. 2007; Massi & Jaron 2013), and/or by a neutron star in the propeller regime (Wang & Robertson 1985).

So far, seven systems have been confirmed as  $\gamma$ -ray binaries - PSR B1259-63 (Aharonian et al. 2005a), LS 5039 (Aharonian et al. 2005b), LS I +61 303 (Albert et al. 2006), HESS J0632+057 (Aharonian et al. 2007), 1FGL J1018.6-5856 (Corbet et al. 2011), PSR J2032+4127 (Lyne et al. 2015) and LMC-P3 (Corbet et al. 2016). The nature of the compact object is already known in PSR B1259-63 and PSR J2032+4127, where radio observations confirm that they contain neutron stars (Johnston et al. 1992; Abdo et al. 2009). Based on the donor star and the presence of a circumstellar disc, two subgroups of  $\gamma$ -ray binaries are proposed. The first subgroup harbours an O-type donor star and shows a single-peak profile in their  $\gamma$ -ray light-curve. The second subgroup contains an OBe star and shows several peaks in their light-curves, occasionally correlated with the

times when the compact object crosses and in some cases truncates the circumstellar disc of the donor star (Paredes & Bordas 2019).

MWC 148 (HD 259440) was identified as the optical counterpart of the variable TeV source HESS J0632+057 (Aharonian et al. 2007) and also detected in the GeV domain (Li et al. 2017). The system consists of a B0Vpe star (Casares et al. 2012) and a compact object, with an orbital period  $P_{\text{orb}} = 315_{-4}^{+6}$  d (Aliu et al. 2014).

MWC 656 (HD 215227) is the suspected optical counterpart of the  $\gamma$ -ray source AGL J2241+4454 detected by the *AGILE* satellite above 100 MeV (Lucarelli et al. 2010; Williams et al. 2010). It is the first discovered binary containing a black hole as a companion of a Be star (Casares et al. 2014). MWC 656 was only occasionally detected at GeV energies (Aleksić et al. 2015). The black hole nature of the compact object renders it similar to the typical  $\gamma$ -ray binaries. The orbital period of the system, obtained by optical photometry and later confirmed by radial velocity measurements, is  $P_{\text{orb}} = 60.37 \pm 0.04$  d (Williams et al. 2010; Casares et al. 2014).

Here, using photometric and spectral observations, we estimate the rotational period, the radius and the inclination of the mass donors in the Be/ $\gamma$ -ray binaries MWC 148 and MWC 656.

## 2 Observations

We use both space photometry and ground-based spectra.

\* Data from TESS and Rozhen

\*\* Corresponding author: rkz@astro.bas.bg

**Table 1** Spectroscopic observations of MWC 148 and MWC 656. In the table are given the date of observations, UT start, exposure time in seconds, signal-to-noise ratio at about 6600 Å, EW( $H\alpha$ ), FWHM( $H\alpha$ ), EW(FeII5316), and FWZI(FeII5316).

Object	Date-obs yyyy-mm-dd:hh:mm	exp-time [sec]	S/N	EW( $H\alpha$ ) [Å]	FWHM( $H\alpha$ ) [km s <sup>-1</sup> ]	EW(FeII5316) [Å]	FWZI(FeII) [km s <sup>-1</sup> ]
MWC 148	2019-02-20T18:45	2400	75	-46.9	411	-0.59	672
MWC 148	2019-12-06T01:45	2400	95	-46.4	405	-0.60	711
MWC 148	2020-01-16T21:16	3600	70	-44.8	418	-0.59	683
MWC 148	2020-09-06T02:01	1800	60	-43.7	412	-0.57	709
MWC 656	2019-08-22T20:10	3600	90	-20.9	493	-0.48	705
MWC 656	2019-12-05T17:48	2400	100	-21.6	491	-0.54	722
MWC 656	2020-09-05T21:50	3600	64	-21.7	490	-0.60	700

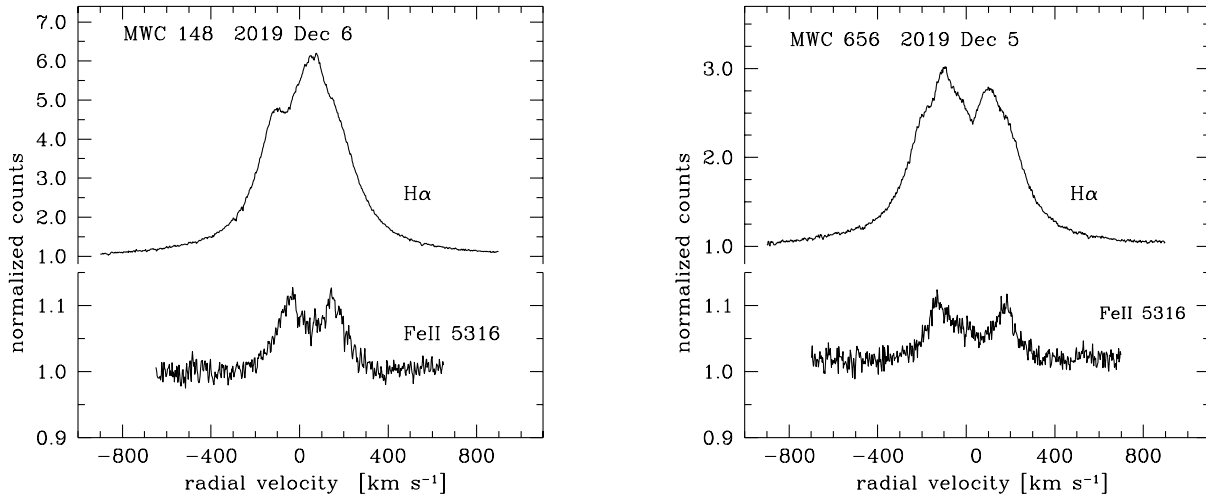


**Fig. 1** The emission lines  $H\alpha$  and FeII 5316 in the spectra of MWC 148 (left panel) and MWC 656 (right panel).

## 2.1 TESS photometric data

The *Transiting Exoplanet Survey Satellite* (*TESS*, Ricker et al. 2015) is a space-based optical telescope launched in 2018 with the primary mission to perform an all-sky survey to search for transiting exoplanets. In order to fulfill the mission, the sky is divided into a number of *sectors*, each of which corresponds to the total field of view of all four cameras of the telescope –  $24^\circ \times 96^\circ$ . Each sector is observed for approximately 27 days at a cadence of 2 minutes. Simple aperture photometry is applied to each of the data files to obtain a barycentered light curve file of the selected object. The bandpass of *TESS* is centered on the classical  $I_c$  filter, but it is wider and spans from 6000 Å to 10 000 Å, in other words the telescope observes the red and the near-infrared emissions of the stars. The light curves of MWC 656 and MWC 148 were downloaded from the Mikulski Archive for Space Telescopes archives<sup>1</sup>.

## 2.2 Rozhen spectral data

The spectral observations were obtained with the ESPERO spectrograph of the 2.0m RCC telescope at Rozhen National Astronomical Observatory located in Rhodope Mountain, Bulgaria. ESPERO is a fiber-fed Echelle spectrograph giving a dispersion of  $0.06 \text{ \AA px}^{-1}$  and resolving power  $\sim 30000$  at 6560 Å (Bonev et al. 2017). The spectral processing and measurements of the spectral lines are performed using standard routines provided by IRAF (Tody 1993). On each spectrum we measure the equivalent width EW( $H\alpha$ ) and the full width at half maximum (FWHM) of the  $H\alpha$  emission line, equivalent width EW(5316) and the full width at zero intensity (FWZI) of the FeII 5316 Å line. FWZI is the full width of the emission line at the continuum level. Examples of the emission lines are presented in Fig. 1. They are normalized to the local continuum. The typical errors of our measurements are  $\pm 5\%$  in EW( $H\alpha$ ),  $\pm 7 \text{ km s}^{-1}$  in FWHM( $H\alpha$ ),  $\pm 10\%$  in EW(FeII5316),  $\pm 40 \text{ km s}^{-1}$  in FWZI(FeII). The log of observations is given in Table 1.

<sup>1</sup> <https://archive.stsci.edu/tess/>

Traces of residual wings due to photospheric absorption were not detected and the interpolated continuum was taken as the baseline during the measurements of EW and FWHM. The equivalent width is measured using *splot* routine in IRAF by marking two continuum points around the line to be measured. The linear continuum is subtracted and the flux is determined by simply summing the pixels with partial pixels at the ends. The method calculates the area under the profile irrespective of its shape (e.g. Mathew & Subramaniam 2011). The FWHM is measured by identifying the points of the emission line profile where the intensity is equal to one half of the peak intensity, as shown in Fig. 1 of Glebocki et al. (1986). The horizontal distance between this two points was measured. This measurement also does not depend on the profile shape.

### 3 Analysis methodology

In this section we give the equations connecting the relevant parameters of the primary components on which our estimates are based. For the Be stars, Hanuschik (1989) gives a relation between projected rotational velocity ( $v \sin i$ ), FWHM( $H\alpha$ ), and EW( $H\alpha$ ). We use his relation in the form  $v \sin i = 0.813 (\text{FWHM } 10^{0.08 \log \text{EW}(H\alpha) - 0.14} - 70)$ , (1) where FWHM and  $v \sin i$  are measured in  $\text{km s}^{-1}$ ; EW( $H\alpha$ ) is in  $\text{\AA}$ .

The Fe II lines are optically thin and their profiles reflect the Keplerian rotation in the innermost part of the Be disc (Hanuschik 1996). The inclination of the Be star is connected with the full width at zero intensity of the FeII lines and its radius:

$$\frac{\text{FWZI}}{2 \sin i} = \left( \frac{GM_1}{(1 + \epsilon)R_1} \right)^{1/2}, \quad (2)$$

where  $G$  is the gravitational constant,  $M_1$  is the mass of the Be star,  $R_1$  is its radius,  $i$  is the inclination of the Be star to the line of sight,  $\epsilon$  is a dimensionless parameter,  $\epsilon \geq 0$ . Eq. 2 represents the Keplerian motion in the disc and is a modification of that used in Sect. 6.1 of Casares et al. (2012). The region where the Fe II lines are produced can be extended down to the very surface of the Be star or close to it. The parameter  $\epsilon$ , for which we adopt  $0 \leq \epsilon < 0.1$ , represents how close to the surface of star the emission at FWZI of the FeII lines is formed.

The rotational period of the Be star is also connected with the above parameters:

$$P_{\text{rot}} = \frac{2\pi R_1}{v \sin i} \sin i. \quad (3)$$

The rotational periodicity is probably due to the interaction between the magnetic field of the Be star and its circumstellar disc or the presence of some physical feature, such as a spot or cloud, co-rotating with the star (Smith, Henry & Vishniac 2006). The rotational periods in the Be/ $\gamma$ -ray binaries are expected to be of order 1 day (Zamanov et al. 2016).

The applied methodology involves the following steps:

1. A periodogram analysis of the TESS data is performed to estimate  $P_{\text{rot}}$ ;
2. The parameter  $v \sin i$  is estimated using Eq. 1 and the data in Table 1;
3. A mass value for the Be star is adopted according to its spectral type;
4. Using Eq. 2 and Eq. 3, the values of  $R_1$  and  $i$  are calculated for the primaries of MWC 148 and MWC 656.

The period-search methods applied to the TESS photometry were the phase dispersion minimization, PDM (Stellingwerf 1978) and the CLEAN algorithm (Roberts, Lehar & Dreher 1987).

### 4 MWC 148

TESS photometry for MWC 148, in the interval JD 2451468.2 – JD 2451490.0, can be accessed under Input Catalogue ID 234929785 and is plotted in Fig. 2. The periodogram analysis is presented in the left panel of Fig. 3, where the PDM statistic ( $\theta$ ) and the CLEAN component amplitude are plotted. Over the entire data set, the analysis yields  $P_{\text{rot}} = 1.0908 \pm 0.0002$  d. The periodogram analysis of the data in the (JD – 2450000) time interval 1468 – 1490 gives a clear period of  $1.09 \pm 0.03$  days, in the interval 1468 – 1477 a clear period of  $1.131 \pm 0.025$  days, and in the interval 1478 – 1490 a clear period of  $1.075 \pm 0.025$  days. A visual inspection of the data gives us the possibility to select the parts of the light curve where this periodicity is most clearly visible. Using days 1468 – 1474, we find 1.156 d, and for days 1479 – 1487 we find 1.101 d. The light curve for days 1468 – 1474 is plotted in the right panel of Fig. 3. We consider that the rotational period of the Be star in MWC 148 is in the range  $1.09 \leq P_{\text{rot}} < 1.16$  d.

Using Eq. 1 and the values given in Table 1, we find  $v \sin i = 272 \pm 5$   $\text{km s}^{-1}$ . Casares et al. (2012) give a spectral type B0Vpe. A B0V star is expected to have on average mass  $M_1 = 15.0 \pm 0.5 M_{\odot}$  (Hohle et al. 2010). For MWC 148, Aragona et al. (2010) derived  $M_1 = 13.2 - 19.0 M_{\odot}$  from spectral model fits, which is in agreement with the adopted  $M_1 = 15.0 M_{\odot}$ . Adopting  $\text{FWZI}(\lambda 5316) \approx 694$   $\text{km s}^{-1}$ , and  $v \sin i = 272$   $\text{km s}^{-1}$ , we find  $i = 40^\circ \pm 2^\circ$  and  $R_1 = 9.2 \pm 0.5 R_{\odot}$ .

It is worth noting for comparison that (i) a B0V star is expected to have  $R_1 = 7.2 R_{\odot}$  (Straizys & Kurilienne 1981); (ii) Casares et al. (2012) give  $\text{FWZI}(\lambda 5018) \sim 1300$   $\text{km s}^{-1}$  and  $v \sin i = 373$   $\text{km s}^{-1}$ ; (iii)  $v \sin i = 430$   $\text{km s}^{-1}$  (Gutiérrez-Soto et al. 2007) and  $v \sin i = 500$   $\text{km s}^{-1}$  (Aragona et al. 2010) are reported for this object.

### 5 MWC 656

TESS photometry for MWC 656 (HD 215227), in the interval JD 2451738 – 2451763, can be accessed under In-

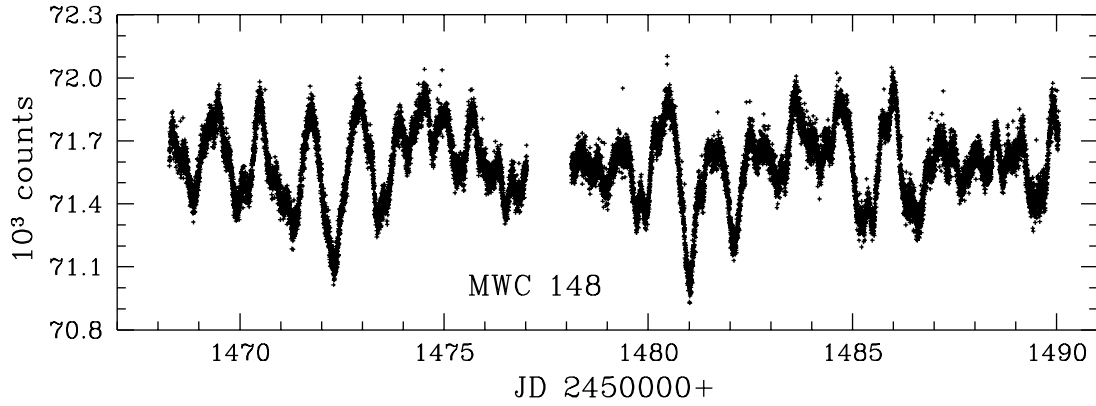


**Fig. 2** TESS light curve of MWC 148.

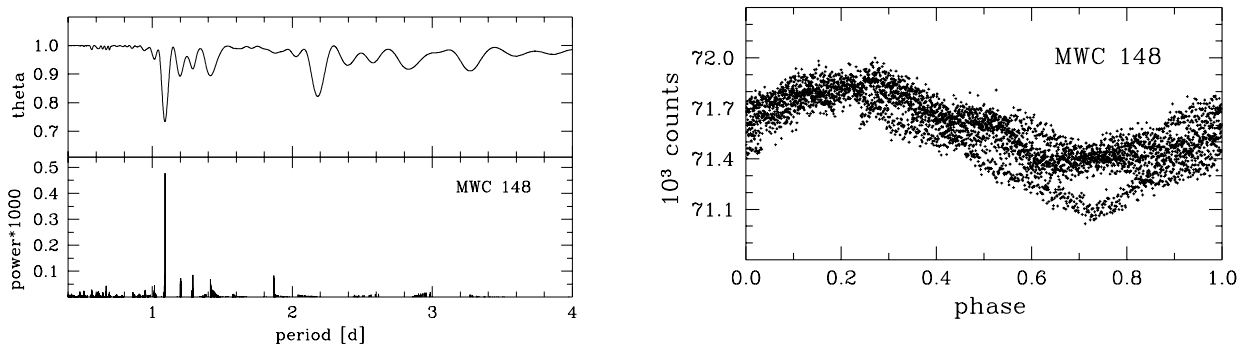


**Fig. 3** Left panel: periodogram analysis for MWC 148 – theta and power versus period. The right panel represents the light curve during 1468 - 1474 folded with a 1.156 d period.

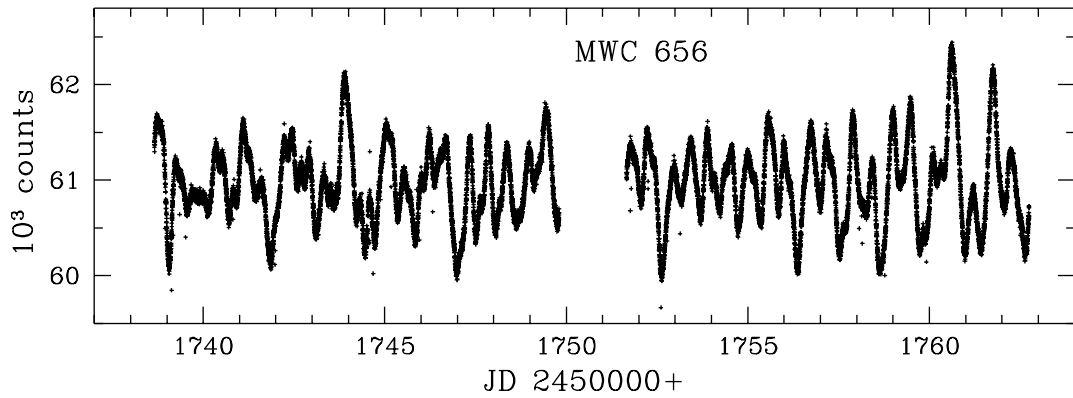


**Fig. 4** TESS light curve of MWC 656.

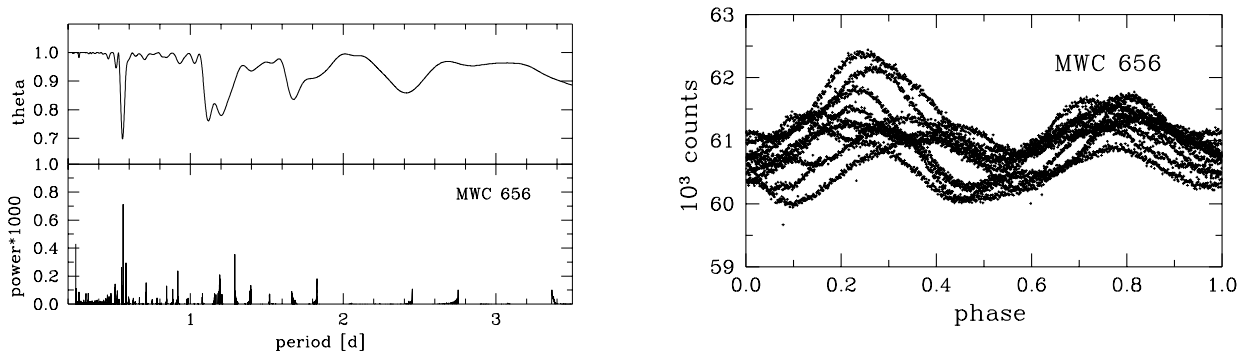


**Fig. 5** Left panel: periodogram analysis for MWC 148. The most significant period is 0.559 days. The right panel represents the light curve during 1751 - 1763 folded with a 1.117 d period, which is probably the rotational period of the B star.

put Catalogue ID 153880067 (Fig. 4). The data gap is due to the telescope being repointed to transfer data to Earth at this time. The periodogram analysis is shown in the left panel of Fig. 5 with the same kind of plots as for the previous source. Over the entire data set, the analysis yields  $P_{\text{rot}} = 0.5586 \pm 0.0002$  d. In contrast, we do not find a clear period in the (JD - 2450000) interval 1738 - 1751 days. However in the interval 1751.6 - 1762.7 days, a clear period of  $0.557 \pm 0.025$  days is detected. Looking at the interval 1760-1763 days, we see that there is a repetition of strong and weak maxima, which probably means that the rotational period is doubled  $P_{\text{rot}} = 1.117$  d.

For the primary, Williams et al. (2010) estimated  $T_{\text{eff}} = 19000 \pm 3000$  K,  $\log g = 3.7 \pm 0.2$ ,  $M_1 = 7.7 \pm 2.0 M_{\odot}$ , and  $R_1 = 6.6 \pm 1.9 R_{\odot}$ . Casares et al. (2014) found that the mass donor is a giant (B1.5-2 III) and gave a mass range 10–16  $M_{\odot}$ . From the results of Hohle et al. (2010), such a star is expected to have  $8.0 < M_1 < 10.0 M_{\odot}$ .

Using the relation between  $v \sin i$ ,  $\text{FWHM}(H\alpha)$ , and  $\text{EW}(H\alpha)$  (Eq. 1), and our values (see Table 1), we find  $v \sin i = 313 \pm 3$  km s<sup>-1</sup>, which is similar to the values  $330 \pm 30$  km s<sup>-1</sup> (Casares et al. 2014),  $262 \pm 26$  km s<sup>-1</sup> (Yudin 2001), and  $330 \pm 50$  km s<sup>-1</sup> (Williams et al. 2010).

We measure  $\text{FWZI}(\text{FeII } 5316) = 12.5\text{-}12.9 \text{ \AA} = 709 \pm 12$  km s<sup>-1</sup>, which is below the value  $\text{FWZI}(\text{FeII } 5018) \sim 1000$  km s<sup>-1</sup> (Casares et al. 2012).

Adopting  $M_1 = 10.0 \pm 0.5 M_{\odot}$ ,  $v \sin i = 313$  km s<sup>-1</sup>, and  $\text{FWZI}(\text{FeII}) = 709$  km s<sup>-1</sup>, the system of Eqs. 2 and 3 can be solved. As a result, we find  $R_1 = 8.8 \pm 0.5 R_{\odot}$  and  $i = 52^{\circ} \pm 2^{\circ}$ . The obtained value of  $R_1$  agrees with the estimates of the average radius for a B1.5-2 III star (8.3–8.8  $R_{\odot}$ , Straizys & Kuriliene 1981).

For MWC 656, from the radial velocity measurements, Casares et al. (2014) obtained  $M_1 \sin^3 i_{\text{orb}} = 5.83 \pm 0.70$ . For  $M_1 = 10 M_{\odot}$ , this gives  $53^{\circ} < i_{\text{orb}} < 60^{\circ}$ . It appears that the orbital plane and the equatorial plane of the Be star are practically coplanar within  $\pm 4^{\circ}$ .

## 6 Discussion

In Be/X-ray binaries the primary is a rapidly rotating Be star with mass  $\sim 10 M_{\odot}$  and the secondary is a neutron star or a black hole. The secondary mass is expected to be  $\sim 2 M_{\odot}$  for a neutron star, and  $\sim 5 M_{\odot}$  in the case of black hole. The orbital periods are in the range 10 – 400 d (Reig 2011). The Be/ $\gamma$ -ray binaries are a subgroup of the Be/X-ray binaries and should have similar binary parameters. They are a product of the evolution of a binary containing two moderately massive stars, which undergoes mass transfer from the originally more massive star towards its companion (Pols et al. 1991; Negueruela 2007). The eccentricities in these systems are caused by a kick to the compact object during the supernova explosion that formed it (e.g. Martin et al. 2009).

HESS J0632+057 (MWC 148) produces non-thermal radio, X-ray, GeV and very high-energy gamma-ray emission. The non-thermal emission is modulated with the 315

days orbital period and has a peculiar light curve containing two peaks, separated by a dip – a sharp peak with a short decay before the apastron passage and a broad (several tens of days) secondary peak after the apastron passage in X-rays and TeV (Aliu et al. 2014, Archer et al. 2020). The non-thermal activity before and around apastron can be linked to (i) the accumulation of non-thermal particles in the vicinity of the binary, and the sudden drop of the emission before apastron is produced by the disruption of the two-wind interaction structure, allowing these particles to escape efficiently (Bosch-Ramon et al. 2017) or (ii) an accumulation of hot shocked plasma in the inner spiral arm, later released when the spiral arm is disrupted in the periastron-apastron direction (Barkov & Bosch-Ramon 2018).

For MWC 148, two solutions for the orbit indicate that it is highly eccentric:  $e = 0.83 \pm 0.08$  (Casares et al. 2012) and  $e = 0.64 \pm 0.29$  (Moritani et al. 2018). In our previous paper (Zamanov et al. 2017), we assumed the value of  $i$ , on the basis of the strong resemblance of the optical emission lines between MWC 148 and the bright Be star  $\gamma$  Cas (Zamanov, Stoyanov & Martí 2016), for which the inclination is  $i = 43^{\circ} \pm 3^{\circ}$  (Poeckert & Marlborough 1978; Clarke 1990). Our result here for MWC 148 ( $i = 40^{\circ} \pm 2^{\circ}$ ) confirms the assumption that one of the reasons for this similarity is the inclination.

MWC 656 is faint in X-rays and it reaches the faintest X-ray luminosities ever detected in stellar-mass black holes (Ribó et al. 2017). It may not continuously emit in  $\gamma$ -rays (Alexander & McSwain 2016). For this binary, Casares et al. (2014) found that the mass of the black hole is in the range 3.8 – 6.9  $M_{\odot}$ . The orbital eccentricity is  $e = 0.10 \pm 0.04$ . It is suggested that the warp and precession observed in Be star discs may be caused by a misalignment between the spin axis of the Be star and the orbit of the binary companion (Martin et al. 2011). Our results indicate that there is no misalignment in MWC 656, and consequently warping and precession should not be observed.

The velocity kick from the supernova has two effects – it renders the orbit eccentric and it misaligns the orbit with respect to the spin axis of the Be star. In systems that experience low velocity kicks, the misalignments tend to be small (Martin et al. 2011). The low orbital eccentricity and the alignment between the spin axis of the primary and the axis of the binary orbit, indicates that the compact object in MWC 656 was born with low kick velocity.

## 7 Conclusions:

We evaluated some parameters for the mass donor stars in the Be/ $\gamma$ -ray binaries MWC 148 and MWC 656. For MWC 148, we estimate  $v \sin i = 272 \pm 5$  km s<sup>-1</sup>,  $P_{\text{rot}} = 1.10 \pm 0.03$  d,  $R_1 = 9.2 \pm 0.5 R_{\odot}$ , and  $i = 40^{\circ} \pm 2^{\circ}$ . For MWC 656, we obtain  $v \sin i = 313 \pm 3$  km s<sup>-1</sup>,  $P_{\text{rot}} = 1.12 \pm 0.03$  d,  $R_1 = 8.8 \pm 0.5 R_{\odot}$ , and  $i = 52^{\circ} \pm 3^{\circ}$ . These parameters should be useful for future accurate modeling of these systems.

*Acknowledgements.* This work is supported by Bulgarian National Science Fund – project KII-06-H28/2 “Binary stars with compact object”. JM acknowledges support by grant PID2019-105510GB-C32 / AEI / 10.13039/501100011033 from the Agencia Estatal de Investigación of the Spanish Ministerio de Ciencia, Innovación y Universidades, and by Consejería de Economía, Innovación, Ciencia y Empleo of Junta de Andalucía as research group FQM- 322, as well as FEDER funds. YMN acknowledges grant DCM 577/17.08.2018 from National Research Programme “Young scientists and postdoctoral students” of the Bulgarian Ministry of Education and Science. We are grateful to Mike Bode (Liverpool John Moores University) for critical reading of the manuscript and the anonymous referee for useful comments.

## References

- Abdo, A. A., Ackermann, M., Ajello, M., et al. 2009, *Science*, 325, 840
- Aharonian, F., Akhperjanian, A. G., Aye, K.-M., et al. 2005a, *A&A*, 442, 1
- Aharonian, F., Akhperjanian, A. G., Aye, K.-M., et al. 2005b, *Science*, 309, 746
- Aharonian, F. A., Akhperjanian, A. G., Bazer-Bachi, A. R., et al. 2007, *A&A*, 469, L1
- Albert, J., Aliu, E., Anderhub, H., et al. 2006, *Science*, 312, 1771
- Aleksić, J., Ansoldi, S., Antonelli, L. A., et al. 2015, *A&A*, 576, A36
- Alexander, M. J. & McSwain, M. V. 2016, *ASP Conf. Ser.*, 506, 243
- Aliu, E., Archambault, S., Aune, T., et al. 2014, *ApJ*, 780, 168
- Aragona, C., McSwain, M. V., & De Becker, M. 2010, *ApJ*, 724, 306
- Archer, A., Benbow, W., Bird, R. et al. 2020, *ApJ*, 888, 115
- Barkov, M. V. & Bosch-Ramon, V. 2018, *MNRAS*, 479, 1320
- Bonev, T., Markov, H., Tomov, T., et al. 2017, *Bulgarian Astronomical Journal*, 26, 67
- Bosch-Ramon, V., Barkov, M. V., Mignone, A., et al. 2017, *MNRAS*, 471, L150
- Casares, J., Negueruela, I., Ribó, M., et al. 2014, *Nature*, 505, 378
- Casares, J., Ribó, M., Ribas, I., et al. 2012, *MNRAS*, 421, 1103
- Chernyakova, M. & Malyshev, D. 2020, *Proceeding of Science*, 362, 045
- Clarke, D. 1990, *A&A*, 227, 151
- Corbet, R. H. D., Cheung, C. C., Kerr, M., et al. 2011, *The Astronomer’s Telegram*, 3221
- Corbet, R. H. D., Chomiuk, L., Coe, M. J., et al. 2016, *ApJ*, 829, 105
- Dubus, G. 2006, *A&A*, 456, 801
- Dubus, G. 2013, *A&A Rev.*, 21, 64
- Glebocki R., Sikorski J., Bielicz E., Krogulec M., 1986, *A&A* 158, 392
- Gutiérrez-Soto, J., Fabregat, J., Suso, J., et al. 2007, *A&A*, 476, 927
- Hanuschik, R. W. 1989, *Ap&SS*, 161, 61
- Hanuschik, R. W. 1996, *A&A*, 308, 170
- Hohle, M. M., Neuhäuser, R., & Schutz, B. F. 2010, *AN*, 331, 349
- Johnston, S., Manchester, R. N., Lyne, A. G., et al. 1992, *ApJ*, 387, L37
- Li J., Torres D. F., Cheng K.-S., et al. 2017, *ApJ*, 846, 169
- Lucarelli, F., Verrecchia, F., Striani, E., et al. 2010, *The Astronomer’s Telegram*, 2761
- Lyne, A. G., Stappers, B. W., Keith, M. J., et al. 2015, *MNRAS*, 451, 581
- Martin, R. G., Tout, C. A., & Pringle, J. E. 2009, *MNRAS*, 397, 1563
- Martin, R. G., Pringle, J. E., Tout, C. A., et al. 2011, *MNRAS*, 416, 2827
- Massi, M. & Jaron, F. 2013, *A&A*, 554, A105
- Mathew, B. & Subramaniam, A. 2011, *Bulletin of the Astronomical Society of India*, 39, 517
- Mirabel, I. F. 2012, *Science*, 335, 175
- Moritani, Y., Kawano, T., Chimasu, S., et al. 2018, *PASJ*, 70, 61
- Negueruela, I. 2007, *ASP Conf. Ser.*, 367, 477
- Paredes, J. M. & Bordas, P. 2019, *Rendiconti Lincei. Scienze Fisiche e Naturali*, 30, 107
- Poeckert, R. & Marlborough, J. M. 1978, *ApJ*, 220, 940
- Pols, O. R., Cote, J., Waters, L. B. F. M., et al. 1991, *A&A*, 241, 419
- Reig, P. 2011, *Ap&SS*, 332, 1
- Ribó, M., Munar-Adrover, P., Paredes, J. M., et al. 2017, *ApJ*, 835, L33
- Ricker, G. R., Winn, J. N., Vanderspek, R., et al. 2015, *Journal of Astronomical Telescopes, Instruments, and Systems*, 1, 014003
- Roberts, D. H., Lehar, J., & Dreher, J. W. 1987, *AJ*, 93, 968
- Romero, G. E., Okazaki, A. T., Orellana, M., et al. 2007, *A&A*, 474, 15
- Smith, M. A., Henry, G. W., & Vishniac, E. 2006, *ApJ*, 647, 1375
- Stellingwerf, R. F., 1978, *ApJ*, 224, 953
- Straizys, V. & Kuriliene, G. 1981, *Ap&SS*, 80, 353
- Tody, D. 1993, *ASP Conf. Ser.*, 52, 173
- Wang, Y.-M. & Robertson, J. A. 1985, *A&A*, 151, 361
- Williams, S. J., Gies, D. R., Matson, R. A., et al. 2010, *ApJ*, 723, L93
- Yudin, R. V. 2001, *A&A*, 368, 912
- Zamanov, R., Stoyanov, K., & Martí, J., 2016, *Bulgarian Astronomical Journal*, 24, 40
- Zamanov, R. K., Stoyanov, K. A., Martí, J., et al. 2016, *A&A*, 593, A97
- Zamanov, R., Martí, J., & García-Hernández, M. T., 2017, *Bulgarian Astronomical Journal*, 27, 57